arXiv:cond-mat/0407490v1 [cond-mat.supr-con] 19 Jul 2004

Dendritic flux avalanches and nonlocal electrodynamics in thin superconducting films

Igor S. Aranson[1], Alex Gurevich[2], Marco S. Welling[3], Rinke J. Wijngaarden[3],
Vitalii K. Vlasko-Vlasov[1], Valerii M. Vinokur[1], and Ulrich Welp[1]
[1]*Materials Science Division, Argonne National Laboratory, Argonne, Illinois 60439*
[2]*Applied Superconductivity Center, University of Wisconsin, Madison, Wisconsin 53706*
[3]*Division of Physics and Astronomy, Faculty of Sciences, Vrije Universiteit, De Boelelaan 1081, 1081HV Amsterdam, The Netherlands*

(Dated: March 22, 2022)

We present numerical and analytical studies of coupled nonlinear Maxwell and thermal diffusion equations which describe nonisothermal dendritic flux penetration in superconducting films. We show that spontaneous branching of propagating flux filaments occurs due to nonlocal magnetic flux diffusion and positive feedback between flux motion and Joule heat generation. The branching is triggered by a thermomagnetic edge instability which causes stratification of the critical state. The resulting distribution of magnetic microavalanches depends on a spatial distribution of defects. Our results are in good agreement with experiments performed on Nb films.

PACS numbers: 74.20.De, 74.25.Qt, 74.25.Fy

Penetration of magnetic flux in a type-II superconductor can result in nonequilibrium pattern formation, such as magnetic macroturbulence [1], kinetic front roughening [2], magnetic microavalanches [3], and dendritic structures [4]. Dendritic flux penetration has been revealed by magneto-optical imaging (MOI) on multiple scales $\sim 1-100\mu$m much greater than intervortex spacings in $YBa_2Cu_3O_7$[5], Nb [6, 7], Nb_3Sn[8], and MgB_2[9]. Similarity of these dynamic flux patterns in different materials indicates a generic collective behavior of vortices.

Recently it has been shown both experimentally and theoretically that dendritic flux penetration is due to a positive feedback between moving flux and the Joule heating coupled by a highly nonlinear voltage-current characteristic [4, 9, 10]. The resulting thermal bistability of current-carrying superconductors gives rise to switching waves between a cold superconducting phase and a hot resistive phase self-sustained by the Joule heating [11]. Dendritic flux penetration in superconductors has analogs in the theory of pattern formation out of equilibrium [12] and instability of solidification fronts [13].

Dendritic flux dynamics in superconductors was observed in numerical analysis of nonisothermal magnetic diffusion in a slab in a parallel field, when flux penetration was triggered by a local heat pulse [10]. However, experiments have been mostly done on films in a perpendicular ramping magnetic field in which case magnetic flux diffusion becomes strongly nonlocal due to long-range interaction of vortices [14]. In this Letter we calculate dendritic flux penetration controlled by nonlocal magnetic flux diffusion coupled to thermal diffusion in thin films. We report a novel *nonlocal* mechanism of flux branching, which captures salient features of dendritic flux penetration in superconducting films.

We consider a thin film strip of the width w along the y-axis and thickness $d \ll w$ in the xy plane perpendicular to the magnetic field H_0. Distributions of the magnetic induction, $\mathbf{B}(\mathbf{r},t)$, and temperature $T(\mathbf{r},t)$ are described by the Maxwell equation coupled to the heat diffusion:

$$C\partial_t T = \nabla\kappa\nabla T - (T-T_0)h/d + \mathbf{JE}(J,T), \qquad (1)$$

$$\partial_t \mathbf{B} = -\nabla\times\mathbf{E}(\mathbf{J},\mathbf{T}), \;\; \nabla\times\mathbf{H} = \mathbf{J}\delta(z). \qquad (2)$$

Here $C(T)$ is the heat capacity, $\kappa(T)$ is the thermal conductivity, $h(T,T_0)$ is the heat transfer coefficient to the coolant or substrate held at the temperature T_0, and $\mathbf{E} = \mathbf{J}E(J,T)/J$ is the electric field, which strongly depends on $T(\mathbf{r},t)$ and the sheet current density $\mathbf{J}(\mathbf{r},t)$.

The $E(J,T,B)$ characteristic accounts for a resistive flux flow state with $E = (J-J_c)\rho_F$ for $J > J_c$ and a low-resistive flux creep state with $E = E_c\exp(J-J_c)/J_1$ for $J < J_c$, where $J_c(T,B)$ is the critical current density. We use the following interpolation formula expressed in terms of observable parameters [10]:

$$E = \rho_F J_1 \ln[1+\exp(J-J_c)/J_1], \qquad (3)$$

where $J_1(T)$ is logarithmic flux creep rate ($J_1 \ll J_c$ below the irreversibility field $B < B^*$), and $\rho_F(T) = \rho_n B/B_{c2}$ is the flux flow resistivity.

We consider weak Joule heating, for which the most essential temperature dependence comes from $E(T)$, while other parameters may be taken at $T = T_0$. The relation between current and the z-component B_z in a film is given by the non-local Biot-Savart law. Expressing $J_x = \partial_y g$ and $J_y = -\partial_x g$ in Eq. (2) in terms of the current stream function $g(x,y,t)$, we obtain the equations for g and the dimensionless temperature θ:

$$\tau\dot{g} = \hat{K}\big[\partial_x[r(j,\theta)\partial_x g + \partial_y[r(j,\theta)\partial_y g] - \tau\dot{H}_0(t)\big], \qquad (4)$$

$$\dot{\theta} = \nabla^2\theta - \theta + \alpha j^2 r(j,\theta). \qquad (5)$$

Here we define the operator $\hat{K}$ in the Fourier space, $\hat{K} = \sum_{\mathbf{k}}\sin(k_x x)\sin(k_y y)g_{\mathbf{k}}/k$, where $k_x = \pi n/L$ and

$k_y = \pi m/w$ with integer m and n to ensure zero normal component of $\mathbf{J}$ at edges of a rectangular film of width w and length L [15]. Furthermore, $\theta = (T - T_0)/(T^* - T_0)$, $J_c(T^*) = 0$, $j = J/J_1 = [j_x^2 + j_y^2]^{1/2}$, $H_z(x,y) = \sum_{\mathbf{k}} \exp(-dk - i\mathbf{kr}) g_{\mathbf{k}} k/2 + H_0(t)$, the factor $\exp(-dk)$ accounts for a finite film thickness, the derivatives in Eqs. (4) and (5) are taken over normalized time t/t_h and coordinates $\mathbf{r}/L_h$, and the nonlinear resistivity $r(j,\theta) = \ln[1 + \exp(j - j_c(\theta))]/j$ is obtained from Eq. (3). Here the thermal length $L_h = (d\kappa/h)^{1/2}$ and time $t_h = Cd/h$ define the spatial scale and the cool down time of $T(\mathbf{r},t)$ at a frozen $\mathbf{J}(\mathbf{r})$. Hereafter we take $j_c(\theta) = j_0(1-\theta)$ for $\theta < 1$, and $j_c = 0$ for $\theta > 1$, and $J_1(T) = \text{const}$ [10], assume that a uniform magnetic field $H_0(t) = \dot{H}_0 t$ is ramped up with the rate $\dot{H}_0$, and neglect the field dependence of J_c. Evolution of $\theta(\mathbf{r},t)$ and $g(\mathbf{r},t)$ is controlled by two dimensionless parameters:

$$\tau = \frac{\mu_0 \sqrt{d\kappa h}}{2\rho_F C}, \qquad \alpha = \frac{\rho J_1^2 d}{h(T^* - T_0)}. \tag{6}$$

Here $\tau = t_m/t_h$ is the ratio of magnetic and thermal diffusion times, and α quantifies the Joule dissipation. Magnetic nonlocality strongly reduces $\tau = \tau_0 d/2L_h$ in a film as compared to $\tau_0 = \mu_0\kappa/\rho_F C$ in the bulk. Indeed, flux diffusion over a distance L_h along a film takes $t_m \sim dL_h/D_m$, while thermal diffusion takes $t_h \sim L_h^2/D_h$, where $D_m = \mu_0/\rho_F$ and $D_h = \kappa/C$. For Nb films with $d = 0.5\mu$m, at 4.2K, ($\kappa \simeq 0.2$W/cmK, $h \simeq 1$W/cm^{2}K, $\rho_n \simeq 3\cdot 10^{-7}\Omega$cm [7], and $C \simeq 2\cdot 10^{-3}$J/cm^{3}K), we obtain $L_h = (d\kappa/h)^{1/2} \simeq 0.03$mm, $t_h = Cd/h \simeq 10^{-7}$s, $d/L_h \sim 10^{-2}$, $\tau \sim 0.1$, with τ decreasing as T_0 increases.

We used Eqs. (4), (5) to study flux penetration in a film with periodic boundary conditions (b.c.) along x and $\partial_y\theta = g = 0$ at $y = 0, w$. Eqs. (4), (5) were solved numerically by a quasi-spectral method based on the Fast Fourier Transform; up to 1024×512 harmonics were used. To implement non-periodic b.c. in the y-direction we used the domain of doubled length with the condition $g(x,y) = -g(x, 2w - y)$. Calculated steady-state distributions of $B_z(x)$ are very close to those of the Bean model [17]. In the majority of numerical runs for $\tau \ll 1$, we observed spontaneous avalanches induced by ramping magnetic field $H_0(t) = \dot{H}_0 t$, starting from a zero field cooled state. We also took into account randomly-distributed macroscopic defects modelled by $j_c(\mathbf{r}) = j_0[1 - \theta - \sum_i q_i \cosh^{-1}(|\mathbf{r} - \mathbf{r}_i|/\xi_0)]$ where q_i, $\mathbf{r}_i$ and ξ_0 determine the strength, the position and the radius of the i-th defect. Extended current-blocking defects have been commonly revealed by the MOI [16].

We start with flux penetration in a film with no macro-defects, Fig. 1 and Movie 1 in [17]. The ramping magnetic field first caused penetration of a stable cold flux front. Then an instability causing *periodic modulations* of temperature and propagation of hot magnetic filaments over the preceding smooth magnetic flux distribution develops at the film edge. Once the first wave of magnetic filaments reaches the central line where the magnetization currents change direction, the filaments widen and start splitting at the ends, similar to that of a slab in a parallel field [10]. At the same time, a second wave of hot filaments start propagating from the film edge mostly between the paths of the filaments of the first wave. The new filaments are wider and exhibit shape distortions due to interaction with preceding filaments. Eventually the film cools down and the flux penetration stops, resulting in a frozen multi-filamentary structure [17].

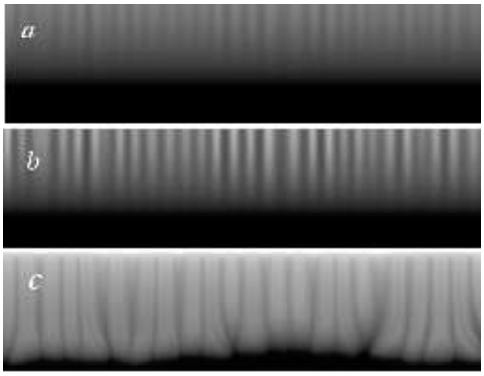


FIG. 1: Temperature distributions in a film with no defects for $\dot{H}_0 = 5J_1/t_h$, $\tau = 0.0025$, $\alpha = 0.008$, system size $600L_h \times 150L_h$ (only quarter part is shown) and $j_0 = 20$ at $t = 16.75t_h$ (a) and $t = 17.75t_h$(b); (c) magnetic flux pattern for $t = 20t_h$

To address the mechanism of the edge instability, we performed a linear stability analysis of steady-state distributions $T(y)$ and $E_0(y)$. Because $E(J,T)$ depends on J and T, linearization of Eqs. (4) and (5) gives two coupled equations for the perturbations $\delta\theta$ and δg, which depend on $E_0(y)$ and $T(y)$. The problem can be simplified by the fact that the flux stratification period ℓ in Fig. 1 is much smaller than the film width w. Because both $E_0(y)$ and $T(y)$ vary on the scale $\sim w$, we can neglect slow variations of $E_0(y)$ and $T(y)$, taking uniform $T = T_0$ and $E_0 = \dot{B}_0 w/2$ at the film edge. Then the solutions, which satisfy the boundary conditions $\delta J_y = \partial_y \delta T = 0$ at the film edge ($y = 0$), take the form $\delta\theta \propto e^{\lambda t + ikx}\cos qy$, and $\delta g \propto e^{\lambda t + ikx}\sin qy$. From Eqs. (4), (5), we obtain the following dispersion relation:

$$(\lambda + 1 + q^2 + k^2 - \beta)(\lambda\tau_i\sqrt{k^2+q^2} + q^2 + sk^2) + q^2\beta(1+s) = 0, \tag{7}$$

where λ and (k,q) are measured in t_h^{-1}, and L_h^{-1}, respectively. The dissipation control parameter $\beta = (dJ/h)\partial E/\partial T$ depends on E_0: if $E(J) = E_c \exp[(J - J_c)/J_1]$ then $\beta \simeq E_0 J_c d|\partial J_c/\partial T|/J_1 h$ for $J < J_c$. The parameter $\tau_i = \mu_0\sqrt{dh\kappa}/2\rho C$, is similar to that in Eq.

(6), except that ρ_F is now replaced with the differential resistivity $\rho(E) = \partial E/\partial J$, and $s = E/J\rho(E) \simeq J_1/J_c$ is the flux creep rate.

Eq. (7) describes coupled thermal and magnetic diffusion modes, the factor $\sqrt{k^2+q^2}$ accounting for the magnetic nonlocality. Positive eigenvalues $\lambda(k,q)$ correspond to unstable modes resulting in spontaneous thermomagnetic structures [18]. For slow flux diffusion $\tau \gg 1$, thermal perturbations with $\lambda \simeq \beta - 1 - k^2 - q^2$ are unstable above the thermal runaway threshold, $\beta > 1$. In this case λ is maximum at $k = q = 0$ so no periodic structures are expected. A completely different situation occurs for fast flux diffusion $\tau \ll 1$ for which Eq. (7) yields

$$\lambda = \beta - 1 - q^2 - k^2 - \frac{q^2\beta(1+s)}{q^2 + sk^2}. \qquad (8)$$

The spectrum of q is determined by the full set of boundary conditions in the theory of flux jumps [19]. For further qualitative analysis we take $q \simeq \pi/2b$, where $\delta J_x(x,b) = 0$, $b = [1 - 1/\cosh(B_0/B_p)]w/2$ is the width of the flux penetrated critical state region, and $B_p = \mu_0 J_c/\pi$ [20]. For a given q, the increment $\lambda(q,k)$ passes through a maximum at the wave vector k_m, which defines the period $\ell = 2\pi/k_m$ of the fastest growing thermomagnetic structure along the film. Here $sk_m^2 = [q^2\beta s(1+s)]^{1/2} - q^2$, thus $\lambda(k,q)$ is maximum at the finite k_m if $\beta > \beta_i = q^2/s(1+s)$, or $\dot B_0 > \dot B_i$. For $s \ll 1$, we obtain $\dot B_i$ and ℓ in normal units:

$$\dot B_i = \frac{\pi^2\kappa}{4b^3|\partial J_c/\partial T|}, \qquad \ell^2 \simeq \frac{16b^2 s}{(\dot B_0/\dot B_i)^{1/2} - 1}. \qquad (9)$$

The period ℓ decreases as $1/s$ and $\dot B_0$ increase, in agreement with our numerical results [17]. The branching instability with $k_m > 0$ and Re $\lambda(\beta_c, k_m, q) > 0$ occurs at $\beta = \beta_c$ in Eq. (8), that is, $\dot B_0 > \dot B_c = hJ_1\beta_c/dbJ_c|\partial J_c/\partial T|$, where

$$\beta_c^{1/2} = (1+2q^2)^{1/2} + q\sqrt{1+1/s}. \qquad (10)$$

For $\tau_i \ll 1$, Eq. (10) gives $\beta_c > \beta_i$ for all $q(t) = \pi/2b(t)$, so a thermomagnetic structure with the finite period $\ell(\beta_c) \ll b$ develops as the width $b(t)$ exceeds b_c, where $\dot B_0 = \dot B_c(b_c)$. Notice that Eq. (7) defines a region $\tau_1 < \tau < \tau_2$ in which λ is complex, which manifests itself in temporal oscillations of growing flux structures.

Next we consider dendritic flux penetration initiated by macroscopic defects, both at the film edge and in the bulk. Such defects can trigger local flux jumps even if the critical state in the bulk is stable [21] and cause branching instability of flux filaments in a slab in a parallel field [10]. Selected results of flux patterns in a film are shown in Fig. 2. For $j_0 = 1/s = 20$ in Fig. 2a, edge defects produce flux fingers superimposed with a smooth flux front. This behavior is characteristic of any superconductor with a highly nonlinear $E(J)$, for which a defect of size ξ_0 produces a much larger disturbance $\simeq \xi_0/s$ across the current flow [22]. The flux fingers widen and split at the ends as they collide with the central line where magnetization currents change direction [10]. As j_0 increases, hot flux filaments in Figs. 2b and 2c get thinner and start branching even *before* they reach the central line. Then new fingers start growing between the defects due to the edge instability considered above, see animations for more details [17]. Moreover, in wider samples (Fig. 2 c, d) the finger undergoes multiple branching giving rise to the characteristic flux dendrites. This new branching mechanism, which was not observed in simulations of flux patterns in a slab [10], is principally due to nonlocal flux diffusion in films. Thinning the filaments as s decreases follows from Eq. (9), while the branching shape instability is facilitated by magnetic nonlocality, which results in a weaker damping of short-wave electromagnetic modes $\lambda_m \propto k$ as compared to local flux diffusion for which $\lambda_m \propto k^2$. Another new effect at higher values of j_0 is a "giant" flux avalanche in Fig. 2c, which starts propagating from the region with no surface defects after the first wave of smaller flux filaments reached the center.

Fig. 2d shows flux patterns in a film with randomly-distributed bulk defects. In addition to the branching due to magnetic nonlocality, propagating flux filaments can undergo splitting caused by local transient heat spikes as they collide with defects. This results in local shape instability of the filaments and their subsequent branching similar to that obtained for local magnetic flux diffusion [10]. With the decrease of j_0 (which is equivalent to an increase of T_0 or H_0 in the experiment) flux filaments become wider and eventually start overlapping, forming a continuous flux front. However, even in this case a significant front roughness still persists both due to a size distribution of individual filaments and due to local heat releases as the flux front collides with defects [17].

The dendritic flux penetration can be regarded as *avalanches* of vortex bundles which do not trigger a global flux jump in the whole sample. Such avalanches produce local temperature spikes, partial flux penetration and a step on magnetization curves $M(B)$ [3, 4]. Nonlocal electrodynamics of films strongly facilitates branching flux propagation, which requires faster magnetic diffusion $\tau = \tau_0\sqrt{dh/\kappa} \ll 1$ characteristic of thin films with $dh \ll \kappa$. Notice that because $b \sim w(B_0/B_p)^2$ for small B_0, both critical ramp rates $\dot B_i \propto B_0^{-6}$ and $\dot B_c \propto B_0^{-6}$ strongly depend on the applied field B_0 for $B_0 \ll B_p$ but level off for $B_0 > B_p$ as $b \to w/2$. Furthermore, both $\dot B_i$ and $\dot B_c$ increase as T_0 increases. Thus, for a given $\dot B_0$, the branching occurs at lower T above a certain field $B_i(T)$, in agreement with many experiments [5, 6, 7, 8, 9].

Fig. 3 shows MOI of flux penetration in two different Nb films in ramping fields. One 9mm×1.8mm×0.5μm Nb film described in detail elsewhere [7] exhibits flux patterns similar to those in Figs. 2a,b where dendritic flux

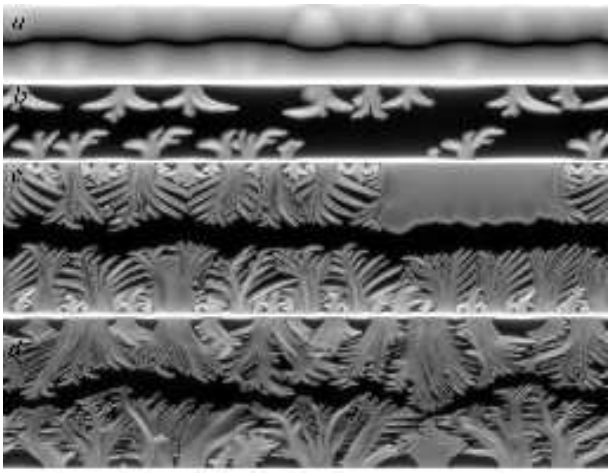


FIG. 2: Flux penetration in a film of $320L_h \times 40L_h$ with 30 random edge defects with $\xi_0 = 0.25L_h$, and amplitudes q_i uniformly distributed between 0 and 0.4, for $\dot{H}_0 = 3J_1/t_h$, $\alpha = 0.08, \tau = 0.0025$ and $t = 25t_h$ for $j_0 = 20$ (a) and $j_0 = 80$. Black and white correspond to the Meissner and vortex phases, respectively; (c) Flux penetration in wide film of $600L_h \times 150L_h$ for $\dot{H}_0 = 5J_1/t_h$, $j_0 = 60$, 20 edge defects. The "giant" avalanche develops in a defect free region; (d) Flux pattern in a film with 500 randomly distributed bulk defects at $j_0 = 80$. See also Movies 2-6 in [17].

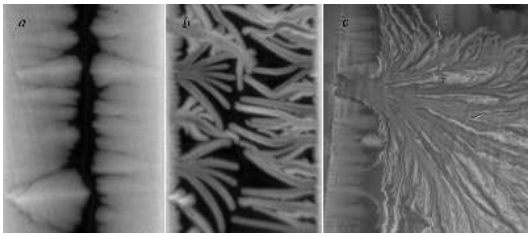


FIG. 3: MOI of flux branching in Nb films of Ref. [7] at T=6.2K and B_0=31.2mT (a) and 4.7K and B_0=36.5mT (b). "Giant flux avalanche" at 4.5K in Nb film of [23] (c). See also Movies 7-8 in [17].

penetration is initiated by surface defects. For this film ($\kappa = 0.2$W/cmK and $h = 1$W/cm^{2}K), we obtain $dh/\kappa \sim 10^{-4}$ and the thermal length $L_h = (d\kappa/h)^{1/2} = 0.03$mm, much smaller than the film width $w = 1.8$mm (i.e. the film width is about $60L_h$ as in Figs. 2a,b), in which case the magnetic nonlocality does play the key role. Fig. 3c shows MOI of an effectively wider (4mm×4mm×0.1μm) film [23] ($w \sim 10^2 L_h$), in which in addition to small microavalanches near the film edge a "giant" avalanche, similar to that triggered by a laser pulse in $YBa_2Cu_3O_7$ [5] and those in Fig. 2c,d develops.

In conclusion, we proposed a mechanism of flux fragmentation in superconducting films caused by coupling of nonlocal flux diffusion with local thermal diffusion.

This work was supported by the NSF MRSEC (DMR 9214707) (AG); US DOE, BES-Materials Sciences (# W-31-109-ENG-38) (IA,VV, VKV,UW); and by Stichting voor Fundamenteel Onderzoek der Materie, which is financially supported by Nederlandse Organisatie voor Wetenschappelijk Onderzoek (MW,RW).

[1] V.K. Vlasko-Vlasov *et al.*, Physica C **222**, 361 (1994); M.R. Koblishka *et al.*, Europhys. Lett. **41**, 419 (1998).
[2] R. Surdeanu *et al.*, Phys. Rev. Lett. **83**, 2054 (1999).
[3] S. Field *et al.*, Phys. Rev. Lett. **74**, 1206 (1995); E.R. Nowak *et al.*, Phys. Rev. B **55**, 11702 (1997).
[4] E. Altshuler and T.H. Johansen, Rev. Mod. Phys. **76**, 471 (2004).
[5] P. Leiderer *et al.*, Phys. Rev. Lett. **71**, 2646 (1993); U. Bolz *et al.*, Europhys. Lett. **64**, 517 (2003); Physica C **388**, 715 (2003).
[6] C.A. Duran *et al.*, Phys. Rev. B **52**, 75 (1995).
[7] M.S. Welling *et al.*, submitted to Physica C, 2004.
[8] I.A. Rudnev *et al.*, Cryogenics, **43**, 663 (2003).
[9] M. Baziljevich, *et al.*, Physica C **369**, 93 (2002); T.H. Johansen *et al.*, Europhys. Lett. **59**, 599 (2002); F.L. Barkov *et al.*, Phys. Rev. B **67**, 064513 (2003).
[10] I. Aranson, A. Gurevich, and V. Vinokur, Phys. Rev. Lett. **87**, 067003 (2001).
[11] A.V. Gurevich and R.G. Mints, Rev. Mod. Phys. **59**, 941 (1987).
[12] M.C. Cross and P.C. Hohenberg, Rev. Mod. Phys. **65**, 851 (1992).
[13] J.S. Langer, Rev. Mod. Phys. **52**, 1 (1980).
[14] E.H. Brandt, Rep. Prog. Phys. **58**, 1465 (1995); A. Gurevich, Int. J. Mod. Phys. B **9**, 1045 (1995).
[15] Because scales of our flux structures are much smaller that the film width, we used a large-k asymptotics of the kernel $\hat{K}$ in the general equation for $g(\mathbf{r}, t)$ by E.H. Brandt, Phys. Rev. B **52**, 15442 (1995).
[16] V.K. Vlasko-Vlasov, G.W. Crabtree, U. Welp, and V.I. Nikitenko, Nato Science Series E: **356**, 205 (1999); D. Larbalestier, A. Gurevich, D.M. Feldman, and A. Polyanskii, Nature **414**, 368 (2001); Ch. Jooss *et al.*, Rep. Prog. Phys. **65**, 651 (2002).
[17] See EPAPS Document No. or http://mti.msd.anl.gov/aran_h1.htm for extensive collection of movies of dendritic flux and temperature patterns.
[18] A.L. Rakhmanov *et al.*, cond-mat/0405446, predicted a similar thermomagnetic fingering instability for local flux diffusion in a slab.
[19] R.G. Mints and A.L. Rakhmanov, Rev. Mod. Phys. **53**, 551 (1981).
[20] E.H. Brandt and M. Indenbom, Phys. Rev. B **48**, 12893 (1993); E. Zeldov *et al.*, *ibid.*, **49**, 9802 (1994).
[21] R.G. Mints and E.H. Brandt, Phys. Rev. B **54**, 12421 (1996); A. Gurevich, Appl. Phys. Lett. **78**, 1891 (2001).
[22] A. Gurevich and M. Friesen, Phys. Rev. B **62**, 4004 (2000).
[23] V.K. Vlasko-Vlasov *et al.*, Phys. Rev. B **69**, 140504 (2004).